Effect of host compositions on the afterglow properties of phosphorescent strontium aluminate phosphors derived from the sol-gel method

I-Cherng Chen and Teng-Ming Chen[a)]
Department of Applied Chemistry, National Chiao Tung University, Hsinchu 30050, Taiwan

(Received 1 December 2000; accepted 10 February 2001)

The effect of compositions of host precursors on the afterglow and phosphorescent decay properties of Eu^{2+}- and Dy^{3+}-coactivated strontium aluminates (SAED) synthesized by a sol-gel process has been investigated. A variety of strontium aluminates such as $Sr_3Al_2O_6$, $SrAl_2O_4$, and $SrAl_{12}O_{19}$ have been identified in the samples prepared from starting precursors with Al/Sr ratios ranging from 1 to 12, respectively. The initial afterglow intensity (I_0) for SAED phases was found to vary with Al/Sr ratio of the sol-gel precursor, with a maximal I_0 appearing in the sample with Al/Sr of 2 in which $SrAl_2O_4$ dominated. The afterglow decay rate was found to be fastest for sample with Al/Sr ratio of 1:1 in which $Sr_3Al_2O_6$ phase dominated. Moreover, the afterglow decay rates for those with Al/Sr ratio of 2:1 to 12:1, in which $SrAl_2O_4$ and $SrAl_{12}O_{19}$ dominated, were found to be slow and similar.

I. INTRODUCTION

The $SrAl_2O_4$:Eu^{2+},Dy^{3+} phase with β-tridymite type structure[1] was reported to exhibit long persistent bluish-green phosphorescence and has been considered as a useful green phosphor in the application of luminous watches and clocks.[2–5] Katsumata *et al.* have reported that among the four Eu^{2+}- and Dy^{3+}-coactivated strontium aluminates (SAED) crystals of $SrAl_2O_4$, $SrAl_4O_7$, $SrAl_{12}O_{19}$, and $Sr_3Al_2O_6$, only the first three were found to exhibit long-lasting phosphorescence with emission peaking at wavelengths of 520, 480, and 400 nm, respectively.[4] On the basis of the investigation on the phosphorescence (or afterglow), thermoluminescence, and photoconductivity characteristics of polycrystalline $SrAl_2O_4$:Eu^{2+},Dy^{3+}, Matsuzawa *et al.*[3] suggested a mechanism indicating that the phosphorescence is ascribed to the presence of holes and to the trapping and thermal release of holes by Dy^{3+} ions in the system. Katsumata *et al.* were able to grow Eu^{2+}- and Dy^{3+}-coactivated strontium aluminate crystals with different Sr:Al compositions by floating zone techniques.[4,5] Katsumata *et al.* further investigated the effects of Al/Sr mole ratio (from 2.05 to 2.22) and Dy/Eu mole ratio (from 0 to 3.55) on the phosphorescent properties (i.e., spectra and afterglow characteristics) of $SrAl_2O_4$:Eu^{2+},Dy^{3+} crystals and concluded that λ_{em} of 520 nm attributed to Eu^{2+} ions did not vary with the compositions.[5] On the other hand, Yamamoto *et al.* investigated the mechanism of long phosphorescence of polycrystalline MAl_2O_4:Eu^{2+},R^{3+} (M = Sr, Ca; R = Dy, Nd) phases and reported that long-lasting phosphorescence in both phases is attributed to the $4f^6 5d \rightarrow 4f^7$ transition of Eu^{2+} and to the holes thermally released from the trap levels with optimal depth formed by Dy^{3+} or Nd^{3+} in the band gap of the hosts.[6] Jia *et al.* reported the measurements of phosphorescence and decay dynamics for both $SrAl_2O_4$:Eu^{2+} and $SrAl_2O_4$:Eu^{2+},Dy^{3+} single crystals.[7] Their results indicated that the trapping rate of Dy^{3+} ion is fast with efficiency of ca. 40% at ambient temperature and the decay curve of afterglow is nonexponential and could not be explained simply by thermally activated detrapping processes. Hole transport rate was reported for the first time to be an important factor in persistent phosphorescence.[7] On the other hand, Sakai *et al.* studied the effect of host composition on the phosphorescence for $BaAl_2O_4$:Eu^{2+},Dy^{3+} crystals and concluded that the intensity of afterglow phosphorescence, the trap depth, and the trap density derived from the thermoluminescence curves vary with host compositions.[8] Furthermore, Nakazawa *et al.* measured the depth and the relative density of the traps in a series of $SrAl_2O_4$:Eu^{2+},Ln (Ln indicates rare earths except Pm and Lu) by using a transient luminescence method.[9] They concluded that the observed hole activation energies (or trap depths) are very different across the Ln series and related to the ionization potential and the $4f^n \rightarrow 4^{n-1}5d$ transition energies of divalent ions

a)Address all correspondence to this author.
e-mail: tmchen@cc.nctu.edu.tw

of the series. Recently, Zhang *et al.*[10] reported that long-lasting phosphorescent Ln-activated $SrAl_2O_4:Eu^{2+}$ phases (Ln = Y, La, Ce, Nd, Sm, Gd, Tb, Dy, Ho, Er, Tm, Yb, Lu) could be synthesized via a homogeneous precipitation route and concluded that $SrAl_2O_4:Eu^{2+}$ co-activated with Dy^{3+}, Nd^{3+}, Ho^{3+}, Pr^{3+}, and Er^{3+} ions, respectively, was found to show suitable trap depth and low thermal activation energy. Moreover, Yuan *et al.*[11] reported the long-persistent photoconductivity of $SrAl_2O_4:Eu^{2+},Dy^{3+}$ single crystals and their observations support a hole-trapping model that has been used to interpret the strong afterglow from this material.

Apparently, long-lasting phosphorescent $MAl_2O_4:Eu^{2+},Ln^{3+}$ (M = Ca, Sr, Ba; Ln = rare earth ions) phases have been of great interests and have been actively investigated from the perspectives of both materialistic and mechanistic research. Thus, in an attempt to develop recipes for long-lasting phosphorescent phosphors with higher brightness and longer afterglow characteristics and obtain optimal materials parameters for applications of these materials, we have extended Katamatsu and co-workers' investigations on the effect of host compositions on the afterglow properties of $SrAl_2O_4$:Eu, Dy. In this paper we have identified the host phases in SAED phases synthesized from sol-gel precursors with Al/Sr ratio ranging from 1 to 12 on the basis of the XRD data and we also reported their phosphorescence spectra and afterglow decay rates as functions of excitation wavelengths and host compositions.

II. EXPERIMENTAL

A series of Eu^{2+}- and Dy^{3+}-coactivated strontium aluminates (SAED) with Al/Sr mole ratios of 1, 1.5, 2, 2.5, 3, 3.5, 4, 5, 7, 9, 10, 11, and 12, respectively, were synthesized by sol-gel method without adding fluxes, and the detailed synthetic conditions was reported elsewhere.[12] Briefly, we prepared solution I by dissolving 10 g of aluminum isopropoxide (98%, Strem Chemicals, Newburyport, MA) in 100 ml of 2-methoxyethanol (99%, Merck, Darmstadt, Germany) by refluxing at 110 °C for 1 h. On the other hand, we prepared solution II by dissolving nitrates of Sr, Eu, and Dy (all 99.9%, Aldrich Chemicals, Milwaukee, WI) with stoichiometry of 1:0.05:0.05 in a mixture of 2-methoxyethanol and deionized water in 50:50 v/v proportion. To avoid the hydrolysis of cations alkoxides before mixing, we added 6.5 g of ethyl acetoacetate (EAA) into solution I as a chelating agent before mixing of solutions I and II. Solutions I and II were then well mixed by constant stirring and kept in an ice bath to activate the formation of gels.

Several trial stoichiometries of Sr:Al:Eu:Dy were attempted in the synthesis, and the optimal stoichiometry was reported elsewhere.[12] However, the molar stoichiometry leading to the formation of $SrAl_2O_4$:Eu,Dy adopted in this work is 1:2:0.05:0.05 for Sr:Al:Eu:Dy. The SAED phases with nominal compositions for Sr:Al:Eu:Dy were represented as 1:*x*:0.05:0.05 (*x* ranging from 1 to 12, respectively).

The resulting white gels then were dried at 80 to 120 °C for 5 h, heated at temperature between 500 and 1200 °C for 10–24 h, respectively, and finally reduced at 1300 °C under an atmosphere of 5% H_2/95% N_2 for 1 h to ensure the complete conversion of Eu^{3+} to Eu^{2+}.

The synthetic conditions for all SAED samples investigated in this work are summarized as a flow diagram and shown in Fig. 1. Meanwhile, for the purpose of comparison a specimen with nominal composition of $SrAl_2O_4:Eu_{0.05},Dy_{0.05}$ was also prepared by solid-state reactions from $SrCO_3$, Al_2O_3, Eu_2O_3, and Dy_2O_3 (all 99.9%, Aldrich Chemicals, Milwaukee, WI) at 1300 °C for 24 h in air and reduced under an atmosphere of H_2/N_2 at the same temperature for 1 h.

A small portion (20 mg) of resulting gels was dried at 150 °C and characterized by differential thermal analysis (DTA) by using a Du Pont thermal analysis (TGA) system (Du Pont Instruments, Wilmington, DE) with a heating rate of 5 °C/min. The x-ray diffraction (XRD) profiles for SAED phases were collected by using a MAC Science MXP-3 automatic diffractometer (MAC Science Co., Tokyo, Japan) with a

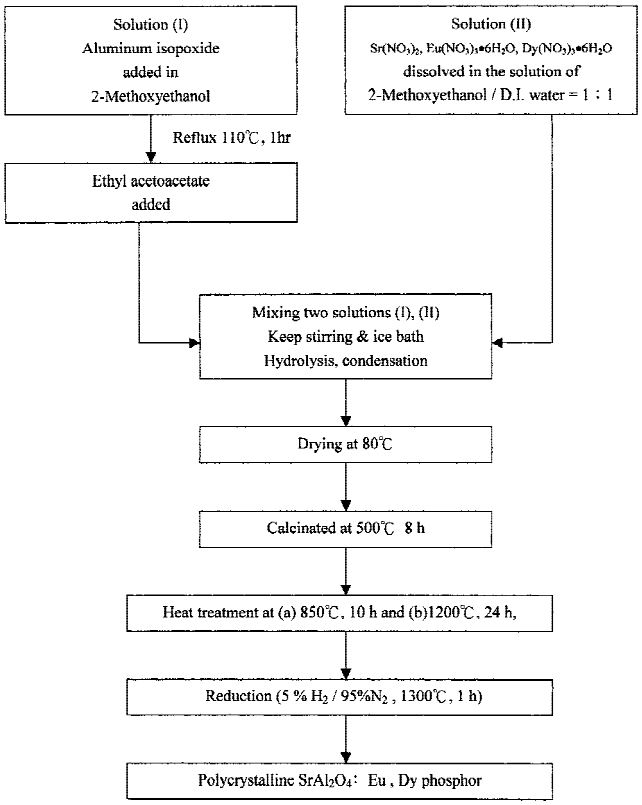

FIG. 1. Flow diagram for the synthesis of $SrAl_2O_4$:Eu,Dy via a sol-gel route.

graphite-monochromatized and Ni-filtered Cu K_α radiation. Special caution was taken to make sure that no starting material or any other impurity phase was identified in the XRD profiles. The morphological investigations of the as-prepared polycrystalline SAED phases were carried out by using a CamScan 4D scanning electron microscope (SEM; CamScan Electron Optics Co., Cambs, U.K.).

Measurements of afterglow curves were performed on a Shimadzu RF-5301PC spectrophotometer (Shimadzu Co., Tokyo, Japan) equipped with a 150-W xenon lamp as an excitation source and a Hamamatsu R928 type photomultiplier (Hamamatsu Photonics, Hamamatsu, Japan) as a detector. The phosphor powders were compacted into a homemade cylindrical dish groove (10 mm diameter × 5 mm length) of a holder that was then transferred to the spectrophotometer. Prior to the measurements of afterglow curves and afterglow decay profiles, the SAED samples were stored in a dark chamber for 8 h to avoid the interference from preactivating light. The SAED samples were then irradiated with ultraviolet with excitation wavelength (λ_{exc}) of 270 and 360 nm for 30 min, respectively. The initial intensity of afterglow defined as I_0 was measured approximately 1 s after the excitation was terminated. Furthermore, the time-dependent afterglow decay intensity (I) for SAED samples, preirradiated with ultraviolet (λ_{exc} = 360 nm) for 30 min, was measured at specified peaking wavelength maxima of afterglow (λ_{AG}) (shown in Table I) in a dark chamber with the excitation source turned off.

III. RESULTS AND DISCUSSION

A. Sol-gel synthesis

As indicated in Fig. 1, the SAED phases can be synthesized via a novel sol-gel route at ca. 1200 °C that is lower than that (i.e., 1400 to 1600 °C) adopted by solid-state reactions without adding fluxes[13,14] or that (1100 to 1500 °C) adopted by synthetic routes with addition of B_2O_3.[15] The addition of ethylacetoacetate into solution I prior to the mixing of solutions I and II was attempted to inhibit the undesirable precipitation of gelatinous $Al(OH)_3$ due to hydrolysis of aluminum isopropoxide by forming metal chelates.[16]

TABLE I. Nominal compositions and host compounds of SAED synthesized from the sol-gel process.

Nominal Al/Sr ratio (Sr:Eu:Dy = 1:0.05:0.05)	Host compounds[a]	λ_{AG} (nm)
1	$Sr_3Al_2O_6$ (85%), $SrAl_2O_4$ (15%)	508
1.5	$Sr_3Al_2O_6$ (50%), $SrAl_2O_4$ (50%)	502
2	$SrAl_2O_4$ (90%), $Sr_3Al_2O_6$ (10%)	492
2.5	$SrAl_2O_4$	490
3	$SrAl_2O_4$ (95%), $SrAl_{12}O_{19}$ (5%)	489
3.5	$SrAl_2O_4$ (90%), $SrAl_{12}O_{19}$ (10%)	490
4	$SrAl_2O_4$ (80%), $SrAl_{12}O_{19}$ (20%)	490
5	$SrAl_{12}O_{19}$ (85%), $SrAl_2O_4$ (15%)	488
6, 7, 8	$SrAl_{12}O_{19}$ (90%), $SrAl_2O_4$ (10%)	488 ± 1
9	$SrAl_{12}O_{19}$ (95%), $SrAl_2O_4$ (5%)	488
10, 11, 12	$SrAl_{12}O_{19}$	488 ± 1

[a]The number in the parentheses indicates the fraction of products.

B. DTA and TGA studies

To study the formation of SAED phases during heat treatment and determine the effective processing conditions for synthesis, we have characterized the products derived from the sol-gel route by differential thermal analysis (DTA) and thermogravimetric analysis (TGA). The DTA and TGA profiles are summarized and shown in Fig. 2. The evaporation of 2-propanol and absorbed water was observed to occur in the range of 80 to 250 °C. Furthermore, there exists an apparent endothermic peak at 595.4 °C that could probably be attributed to the formation of $SrCO_3$ and $Al(OH)_3$ (in minor proportion), as indicated by XRD profile analysis. At higher temperature, a descending curve in the TGA profile was found in the range of 620 to 700 °C that was attributed to the decomposition of $SrCO_3$. In addition, a broad exothermic zone occurring in the range of 800 to 1200 °C in the TGA profile was interpreted as an indication for the formation of the $SrAl_2O_4$ phase.

C. XRD studies and phase identification

Shown in Figs. 3(a)–3(d) are the XRD profiles for $SrAl_2O_4$:$Eu_{0.05}$,$Dy_{0.05}$ derived from sol-gel precursors yet heat treated under the following sintering conditions: (a) at 850 °C for 10 h; (b) at 850 °C for 10 h and then at 1300 °C for 1 h; (c) at 1200 °C for 24 h and then at 1300 °C for 1 h; (d) via the solid-state route at 1200 °C for 24 h and then at 1300 °C for 1 h, respectively. $Sr_3Al_2O_6$ was found in the sample prepared under condition (a), whereas $Sr_3Al_2O_6$ (major) and $SrAl_2O_4$ (minor) were found to dominate in the sample derived from

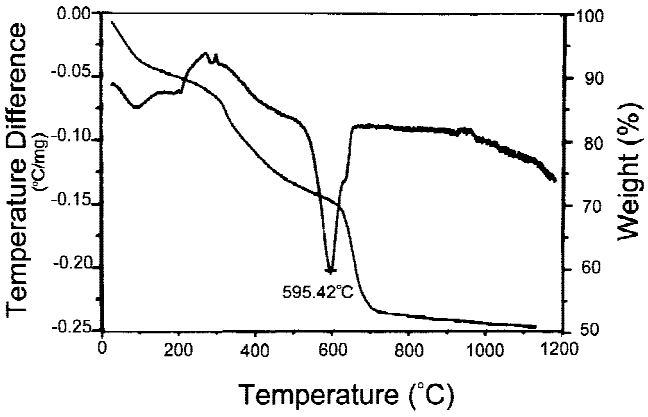

FIG. 2. DTA and TGA profiles of precursors for the synthesis of $SrAl_2O_4$:Eu,Dy via a sol-gel route.

condition (b), as indicated by the XRD profiles represented in Fig. 3. On the contrary, $SrAl_2O_4$ (major) and $SrAl_{12}O_{19}$ (minor) were found in the sample derived from condition (c). In particular, as indicated by the XRD profile shown in Fig. 3(d), the sample synthesized under condition (d) shows the formation of β-tridymite type $SrAl_2O_4$ that exhibits much higher crystallinity than those prepared via the sol-gel route.

The identity of the host for the SAED phases synthesized from the sol-gel process (illustrated in Fig. 1) and the corresponding peaking wavelength of afterglow (λ_{AG}) for SAED derived from precursors with different Al/Sr ratios are summarized in Table I. We have also investigated the effect of Al/Sr ratio on the formation of SAED and the relevant XRD profiles for different SAED phases with nominal Al/Sr molar ratio ranging from 1 to 12 are shown in Figs. 4 and 5, respectively. We have observed that cubic $Sr_3Al_2O_6$[17] (a = 1584.40 pm) dominates as a major phase in the samples with Al/Sr mole ratio of 1 and 1.5 and the monoclinic $SrAl_2O_4$[17] (a = 844.2 pm, b = 882.2 pm, c = 516.07 pm, and β = 93.415°) overwhelms in those with Al/Sr ratio ranging from 1.5 to 7. Moreover, the hexagonal $SrAl_{12}O_{19}$[17] (a = 558.5 pm and c = 220.7 pm) dominates in those with Al/Sr ratio ranging from 4 to 12. Apparently, these observations indicate the complexity of the phase equilibrium in the $SrO–Al_2O_3$ system at elevated temperatures[18] and the sensitivity of stoichiometry of the starting precursors to the formation of $SrAl_2O_4$:Eu^{2+},Dy^{3+} and other SAED phases.

D. Comparison of microstructure

The SEM micrographs for SAED phases derived from the sol-gel route and from a solid-state route are compared and shown in Fig. 6, respectively. As indicated in Fig. 6(a), irregularly spherical grains with size of several tenths of a micron to several microns were

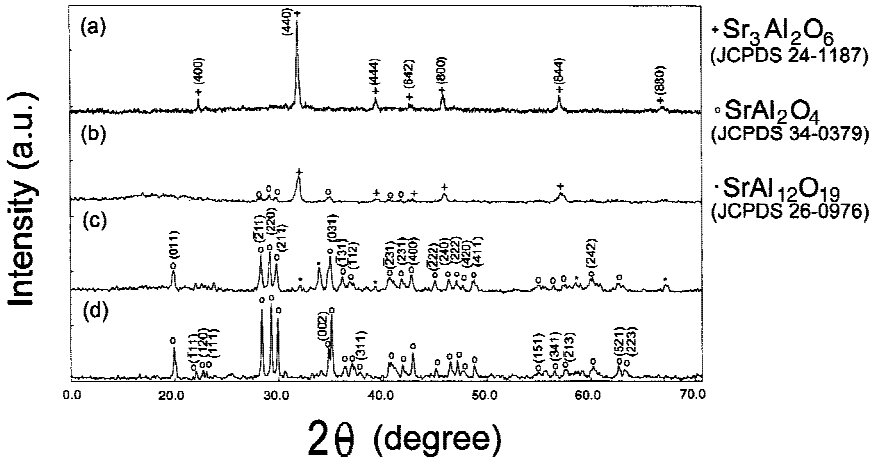

FIG. 3. XRD profiles for sol-gel derived $SrAl_2O_4$:$Eu_{0.05}$,$Dy_{0.05}$: (a) 850 °C for 10 h; (b) 850 °C for 10 h and 1300 °C for 1 h; (c) 1200 °C for 24 h and 1300 °C for 1 h; (d) via a solid-state route at 1300 °C for 24 h.

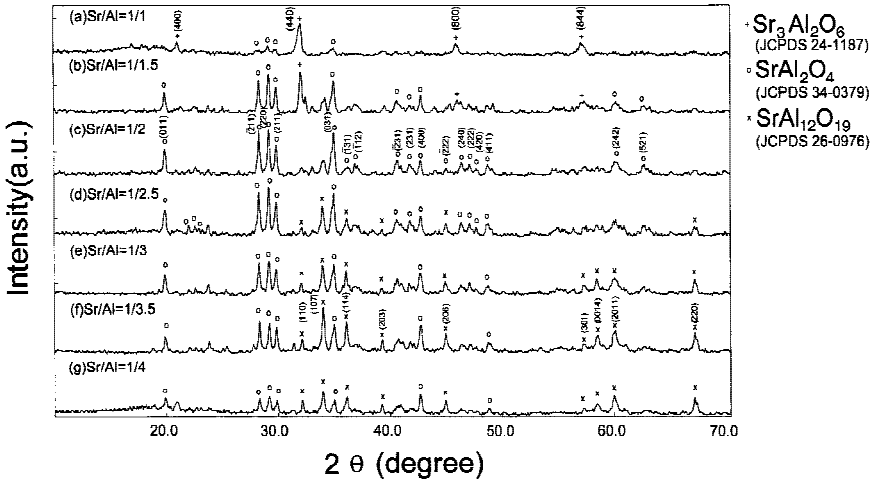

FIG. 4. XRD profiles of SAED phases prepared via sol-gel route with Al/Sr molar ratio from 1 to 4.

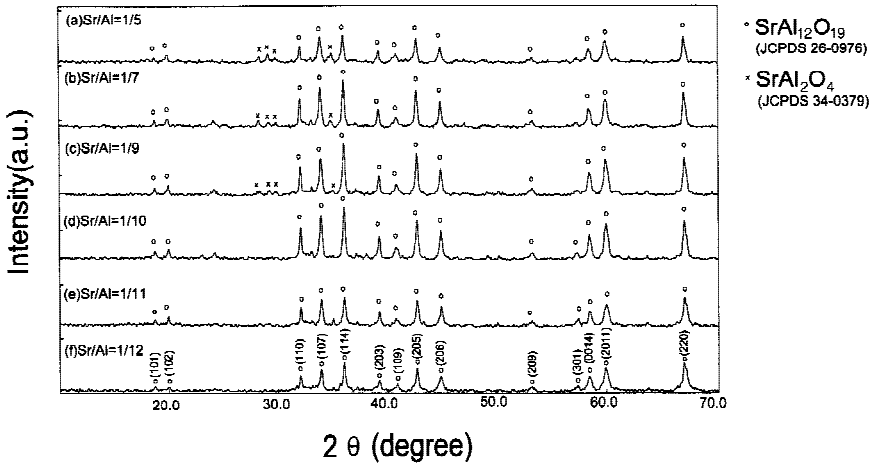

FIG. 5. XRD profiles of SAED phases prepared via sol-gel route with Al/Sr molar ratio from 5 to 12.

observed in the sol-gel derived SAED phases. On the other hand, still irregular yet larger grains were found in the specimen prepared via a solid-state route. We did not observe a great difference in both the grain size and morphology for the SAED phases synthesized from different routes.

E. Afterglow curves and afterglow decay rate

As indicated in Table I, the peaking wavelengths of broad afterglow band (λ_{AG}), attributed to the typical $4f^6 5d^1 \rightarrow 4f^7$ transition of Eu^{2+}, was found to increase systematically from 488 nm (Al/Sr = 8 to 12) to 508 nm (Al/Sr = 1) with decreasing Al/Sr molar ratio. Furthermore, the afterglow curves for SAED phases derived from the solid-state route with Al/Sr ratio of 2 and from gel precursors with different Al/Sr ratios (i.e., 1, 2, and 12) are represented and compared in Fig. 7, respectively. The host of SAED phases has also been identified on the basis of the XRD profile analysis and shown in Table 1 to rationalize the dependence of λ_{AG} on the Al/Sr molar ratio. As shown in Fig. 7, the observed λ_{AG}'s for SAED phases derived from sol-gel synthesis [Figs. 7(b)–7(d)] were found to be significantly shorter than that (i.e., 520 nm) observed for the $SrAl_2O_4$:Eu^{2+},Dy^{3+} phase by Matsuzawa *et al.*[3] The observed discrepancy may be attributed to the phase distribution in the SAED series or the fraction of long-lasting phosphorescent $SrAl_2O_4$:Eu^{2+},Dy^{3+} present in different SAED phases described above.

In addition, the Eu^{2+} ion was considered to distribute randomly in the host lattice of miscellaneous SAED phases (i.e., $SrAl_2O_4$, $SrAl_{12}O_{19}$, and $Sr_3Al_2O_6$) and, thus, the luminescence attributed to Eu^{2+} is the result of interaction in different crystal fields. As indicated by the structural studies on the β-tridymite type $SrAl_2O_4$ by Schulze *et al.*,[1] the Sr^{2+} ions were found to be situated in the interstitials of the framework composed of $(AlO_4)^{5-}$

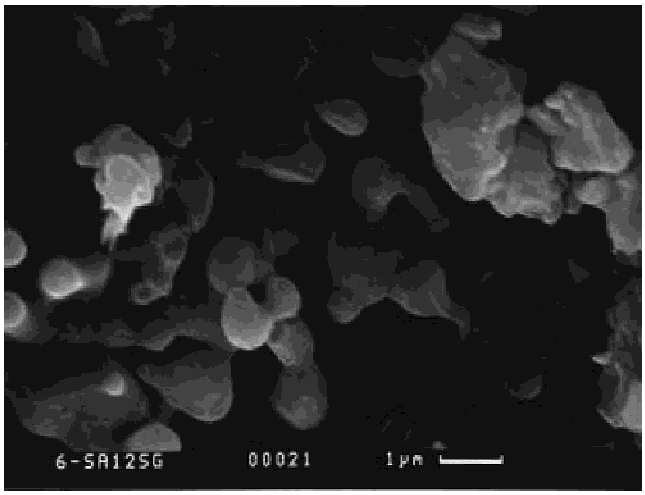

(a)

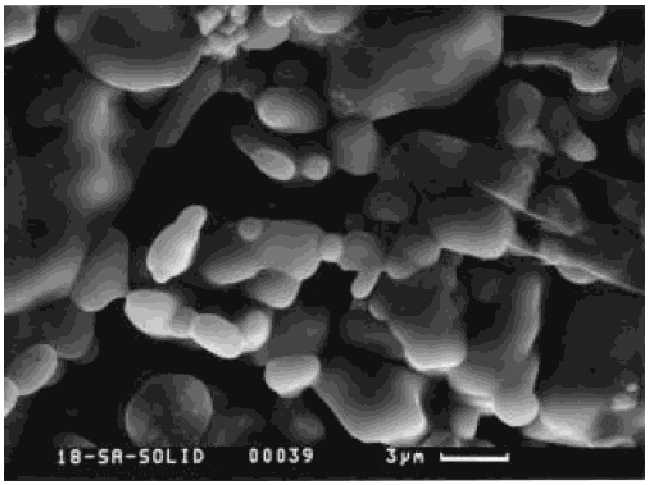

(b)

FIG. 6. Comparison of SEM micrographs for SAED phases synthesized via the (a) sol-gel route and (b) solid-state route.

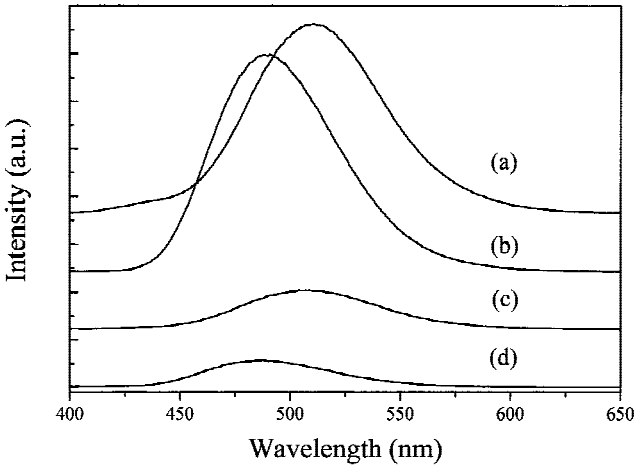

FIG. 7. Afterglow curves for SAED synthesized via (a) the solid-state method and via the sol-gel route with Al/Sr mole ratios of (b) 2, (c) 1, and (d) 12.

tetrahedra that allow for accommodation of ions having a large radius. There are two distinct crystallographic sites occurring in equal multiplicity available to Sr^{2+} that are both coordinated by nine oxygen ions.[1] Monoclinic $SrAl_2O_4$ is considered to be a good host to accommodate Eu^{2+} since the radius of Sr^{2+} is similar to that of Eu^{2+} yet slightly smaller than that of Dy^{3+}. Furthermore, the hole traps ascribed to Sr^{2+} vacancies and defects present in the $SrAl_2O_4$ lattice are commonly generated and stabilized by charge compensation with doping of the Dy^{3+} as an auxiliary activator. Thus, the intensity of afterglow is expected to be highly dependent on the content or relative fraction of $SrAl_2O_4$:Eu^{2+},Dy^{3+}, $SrAl_4O_7$:Eu^{2+},Dy^{3+} (not observed in this work), and $SrAl_{12}O_{19}$:Eu^{2+},Dy^{3+} phases since only these three SAED phases were found to exhibit apparent afterglow behavior.[4]

The observed discrepancy in the shifting of λ_{AG}'s among the three SAED phases may probably be attributed to the difference in the strength of crystal field for Eu^{2+} ions located in different environments, which were inherited from different preparation routes. The $SrAl_2O_4$:Eu^{2+},Dy^{3+} synthesized from the sol-gel processes was found to be less crystalline than that prepared by solid-state reactions, as indicated by the XRD profiles shown in Figs. 3(c) and 3(d). Therefore, the variation of Eu^{2+} coordination environment and the difference in strength of crystal field for Eu^{2+} ion in SAED are considered to be significant to influence the observed λ_{AG}'s qualitatively. Our speculations are verified by the observed λ_{AG}'s values of 513, 492, 508, and 488 nm for $SrAl_2O_4$:Eu^{2+},Dy^{3+} [from the solid-state route, Fig. 7(a)] and three SAED phases synthesized from gel precursors with Al/Sr ratio of 2, 1, and 12, as indicated by Figs. 7(b)–7(d), respectively. The $4f^6 5d$ state of Eu^{2+} has been known to be very sensitive to the change of crystal field strength, and thus, it tends to be easily split into sublevels depending on the strength of the crystal field.[19,20] When Eu^{2+} substitutes Sr^{2+}, the anions experience different field strength in the two Sr^{2+} sites. The energy levels of $4f^6 5d$ state are perturbed by different degrees, resulting in different energy separations between ground and excited states. Furthermore, with increasing crystal field strength the luminescence from these sublevels can vary from blue to red in the visible spectral region.

Regarding the afterglow mechanism for $SrAl_2O_4$:Eu^{2+},Dy^{3+}, the Dy^{3+}codopant is suggested to promote the formation of hole traps in $SrAl_2O_4$:Eu^{2+} in which the activator of Eu^{2+} acts as a luminescent center by exhibiting the $4f^6 5d-4f^7$ broad band luminescence.[3] Ohta *et al.*[21] suggested that the hole traps could be ascribed to the presence of Sr^{2+} defects in the host that are stabilized by charge compensation with Dy^{3+} doping. On the other hand, an electron trap propably originates from oxygen defects that were generated by heating the SAED phases in a reducing atmosphere. In this work we have found that the trapping effect of Dy^{3+} becomes efficient with samples heated at 1300 °C for 1 h under a 5% H_2/95% N_2 atmosphere.

With the Dy^{3+} coactivator composition fixed at 0.05 relative to that of Sr^{2+}, we have observed that the initial afterglow intensity (I_0) for SAED phases varied with the Al/Sr ratio; that is, if one starts from Al/Sr ratio of 1, I_0 increases and reaches a maximum at Al/Sr ratio of 2 and then I_0 decreases drastically in samples with Al/Sr greater than 4. Our results are inconsistent with those reported by Katsumata *et al.*,[5] who indicated that, other than doped Dy^{3+} concentration, the apparent afterglow intensity did not vary with composition for single crystals of $SrAl_2O_4$:Eu^{2+},Dy^{3+} with Al/Sr ratio ranging from 2.05 to 2.22. These discrepancies may be rationalized by considering the phase distribution in SAED, especially the fraction of long-lasting phosphorescent $SrAl_2O_4$:Eu^{2+},Dy^{3+} present in SAED phases synthesized from precursors with different starting Al/Sr ratios, as indicated by Table I. Furthermore, the range of Al/Sr ratio (i.e., from 1 to 12) adopted in our work to synthesize the SAED phases was much wider than those (i.e., from 2.05 to 2.22) investigated in the work of Katsumata *et al.*[4]

The afterglow decay as functions of Al/Sr ratio and excitation wavelength (λ_{exc}) for SAED phases, respectively, was investigated, and the results are shown in Fig. 8. As the Al/Sr ratio varies from 1 to 12, the individual I_0 was observed to increase and reach a maximum at Al/Sr ratio of 2 to 3 and then to drop drastically for λ_{exc} of 270 and 360 nm, respectively. However, considering the excitation efficiency of ultraviolet induced afterglow in the SAED phases with a given Al/Sr ratio, we have found that the λ_{exc} of 270 nm appeared to be more efficient than that of 360 nm.

The decay rate of persistent phosphorescence (afterglow) intensity was investigated and represented in Fig. 9 by plotting reduced intensity $\log(I/I_0)$ against time for SAED phases derived from gel precursors with different Al/Sr ratios. For a given time the $\log(I/I_0)$ was found to increase with increasing Al/Sr ratio, as indicated by the decay rate curves shown in Fig. 9. The decay rate of afterglow was found to be fastest for the sample with Al/Sr ratio of 1:1, in which $Sr_3Al_2O_6$ dominated, whereas that for samples with the Al/Sr ratio in the range of 2:1 to 12:1, in which $SrAl_2O_4$ and $SrAl_{12}O_{19}$ dominated, was found to be similarly slow. Interestingly, the decay rates are similar for SAED phases exhibiting different crystallinity, regardless whether the samples were prepared by the solid-state or sol-gel method.

The decay process of $SrAl_2O_4$:Eu^{2+},Dy^{3+} was reported to be complicated and considered to consist of three regimes by Katamatsu *et al.*[4,5] and Jia *et al.*[7] However, the analysis of the phosphorescence decay process observed in this work is even more complicated by observing the presence of several SAED phases in the hosts, derived from various starting Al/Sr ratios ranging from 1 to 12 in the gel precursors, as revealed in Table I. Unless the relative fraction of each SAED phase present in the hosts can be determined unambiguously, our analysis on the phosphorescence decay mechanism will be extremely difficult if not impossible.

Furthermore, the afterglow decay curves observed in our work appear to indicate different modes of decay mechanisms in different time ranges that could be attributed to the presence of hole traps with different depths and/or, presumably, to the different densities of the traps.[9] Furthermore, whether the decay curves can be deconvoluted and fitted with an equation consisting of three exponential terms from which decay lifetimes are derived[4,5] is currently under investigations in our group.

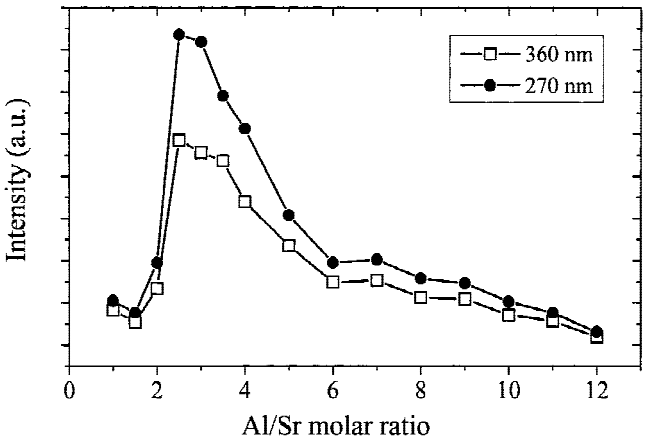

FIG. 8. Initial afterglow intensity (I_0) for SAED observed as a function of Al/Sr ratio and λ_{exc}.

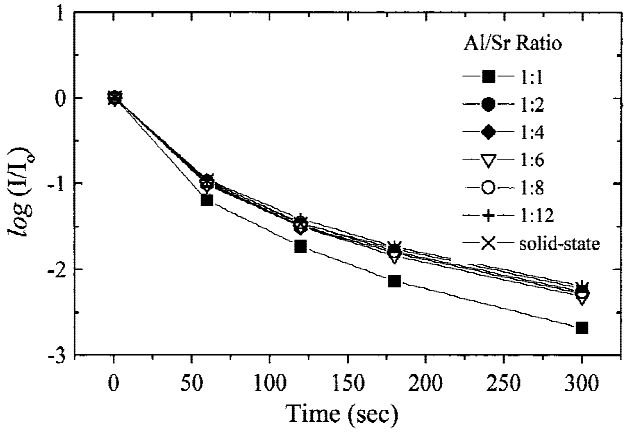

FIG. 9. Comparison of afterglow decay rate for SAED phases synthesized from precursors with different Al/Sr mole ratios (λ_{exc} = 270 nm).

IV. CONCLUSIONS

We have demonstrated a successful synthesis of a series of Eu^{2+}- and Dy^{3+}-coactivated long phosphorescent SAED phases from the precursors with different starting Al/Sr stoichiometries via a novel sol-gel route. The effects of host composition and excitation wavelength on the afterglow properties for the SAED phases were systematically investigated. The phase equilibria for the formation of SAED phases were investigated on the basis of XRD profile analysis. The initial afterglow intensity (I_0) for SAED phases was found to vary with Al/Sr ratio (i.e., from 1 to 12), with a maximal I_0 appearing in the sample with Al/Sr of 2. The afterglow decay rate was also found to be fastest for the sample with Al/Sr ratio of 1:1, whereas that for SAED with other Al/Sr ratios are all similarly slowly. However, the mechanism of afterglow decay process is complicated and difficult to analyze unambiguously due to the presence of various SAED phases in the host.

ACKNOWLEDGMENTS

We are grateful to the National Science Council of Taiwan, Republic of China, for financial support under Contract Nos. NSC88-2113-M-009-013 and NSC89-2113-M-009-024. I-C.C. thanks the Industrial and Technology Research Institute (ITRI) of Taiwan for part of the research facility support. Our thanks are also extended to Dr. Yih-Song Jan for using reduction furnaces and Mr. Kai-Liang Shieh for SEM measurements.

REFERENCES

1. V.A-R. Schulze and Hk. Müller-Buschbauch, Z. Anorg. Allg. Chem. **475,** 205 (1981).
2. Y. Murayama, N. Takeuchi, Y. Aoki, and T. Matsuzawa, U.S. Patent 5 424 006 (1995).
3. T. Matsuzawa, Y. Aoki, N. Takeuchi, and Y. Murayama, J. Electrochem. Soc. **143,** 2670 (1996).

4. T. Katsumata, T. Nabae, K. Sasajima, S. Kumuro, and T. Morikawa, J. Am. Ceram. Soc. **81,** 413 (1998).
5. T. Katsumata, T. Nabae, K. Sasajima, S. Kumuro, and T. Morikawa, J. Electrochem. Soc. **144,** L243 (1997).
6. H. Yamamoto and T. Matsuzawa, J. Lumin. **72–74,** 287 (1997).
7. W. Jia, H. Yuan, L. Lu, H. Liu, and W.M. Yen, J. Lumin. **76, 77,** 424 (1998).
8. R. Sakai, T. Katsumata, S. Komuro, and T. Morikawa, J. Lumin. **85,** 149 (1999).
9. E. Nakazawa and T. Mochida, J. Lumin. **72–74,** 236 (1997).
10. T. Zhang and Q. Su, J. Soc. Inform. Display **8,** 27 (2000).
11. H.B. Yuan, W. Jia, S.A. Basum, L. Lu, R.S. Meltzer, and W.M. Yen, J. Electrochem. Soc. **147,** 3154 (2000).
12. I-C. Chen and T-M. Chen, J. Mater. Res. **16,** 644 (2001).
13. H. Lange, U.S. Patent 3,294,699 (1966).
14. N.A. Sirazhiddinov and P.A. Arifov, Russ. J. Inorg. Chem. **16,** 40 (1971).
15. R.J. Pet, M. van den Nieuwenhof, and J.P.H.M. Duisters, U.S. Patent 4,795,588 (1989).
16. R. Nass and H. Schmidt, J. Non-Cryst. Solids **121,** 329 (1990).
17. Powder Diffraction File, Card Nos. 24-1187 ($Sr_3Al_2O_6$), 34-0379 ($SrAl_2O_4$), and 26-0976 ($SrAl_{12}O_{19}$), Joint Committee on Powder Diffraction Standards (JCPDS) (1999).
18. Phase Diagrams for Ceramists (American Ceramic Society, Columbus, OH, 1987), Vol. I, Fig. 294, and Vol. VI, Fig. 6427.
19. J.Y. Sun, C.S. Shi, and Y.M. Li, Chin. Sci. Bull. **34,** 703 (1989).
20. J. Qiu, K. Miura, N. Sugimoto, and K. Hirao, J. Non-Cryst. Solids **213, 214,** 266 (1997).
21. M. Ohta, M. Maruyama, T. Hayakawa, and T. Nishijo, J. Ceram. Soc. Jpn. **108,** 284 (2000).